

Pressure-Induced Inclusion of Neon in the Crystal Structure of a Molecular $\text{Cu}_2(\text{pacman})$ Complex at 4.67 GPa

SUPPLEMENTARY MATERIAL

Section A: Experimental details

Section B: Supplementary tables (2)

Section C: Supplementary figures (8)

SI_Movie_1: Conformation of $\text{Cu}_2(\text{L})$ as a function of pressure and Ne inclusion.

A. Experimental Details

Recrystallisation of Dicopper Pacman

The dicopper Pacman complex was synthesised by reported procedures.² Single crystals of dicopper pacman were then recrystallised by slow evaporation in dichloromethane to give large black, rod shaped crystals.

Ambient Pressure Single Crystal X-ray Diffraction

A single crystal measuring $50 \times 50 \times 100 \mu\text{m}^3$ was cut from a larger crystal. Single-crystal diffraction data were collected at ambient pressure and at room temperature and 100 K using synchrotron radiation ($E = 16.5 \text{ keV}$) on Beamline 11.3.1 at the Advanced Light Source.³

High Pressure Single Crystal X-ray Diffraction

An irregular block shaped crystal was cut from the bulk sample measuring *ca.* $70 \times 80 \times 90 \mu\text{m}^3$ and loaded into a BX90 type diamond anvil cell (DAC) along with a ruby sphere for pressure determination. The cell was constructed using Boehler-Almax diamonds with a $500 \mu\text{m}$ culet set in tungsten-carbide backing seats. The gasket material forming the sample chamber was rhenium; its initial diameter was $320 \mu\text{m}$ and its initial thickness was *ca.* $110 \mu\text{m}$. The cell was then gas loaded with neon gas as a hydrostatic medium.

High-pressure single crystal diffraction data were collected on compression of the sample in steps of *ca.* 0.8 GPa from 1.30 to 8.13 GPa using synchrotron radiation ($E = 25 \text{ keV}$) on Beamline 12.2.2 at the Advanced Light Source.⁴ Pressure measurements were performed by the ruby fluorescence method.⁵

Decompression of the sample resulted in degradation of the single crystal into multiple domains, and no discernible diffraction data could be obtained.

Structure Solutions and Refinements

All diffraction data were processed using the Bruker suite of programs.⁶ Data reduction was performed by SAINT⁷ and dynamic masks generated by ECLIPSE⁸ were used to mask shaded detector regions from the cell body in the high-pressure data sets. Absorption and systematic error corrections were applied using SADABS⁹ and space group determinations by analysis of systematic absences were performed using XPREP.¹⁰ The ambient pressure-temperature and low temperature structures were

solved by direct methods (SHELXT)¹¹ and all data refined against $|F|^2$ using SHELXL¹² as part of the OLEX2 graphical user interface.¹³

The 3D coordinates of the ambient pressure-temperature structure were used as a starting model in the first high-pressure structure refinement; all subsequent structures were then modelled on the coordinates of at the preceding pressure. Non-hydrogen and non-metal bond distances in the high-pressure structures were restrained to be similar to those of the ambient temperature and pressure structure. Methyl hydrogen atoms were located in 'circular' difference syntheses carried out about the locus of their possible positions; the orientation of the group was allowed to refine while holding the CH distances and HCH angles fixed to ideal values. Other hydrogen atoms were placed in ideal positions and treated with a riding model.

All non-hydrogen atoms in the ambient pressure structures were refined with anisotropic displacement parameters. Only copper atoms were refined anisotropically in the high-pressure structures to reduce the number of refined parameters and improve the low data to parameter ratio. For the structures at 4.67 GPa and above a non-standard unit cell setting is used (with $\beta < 90^\circ$) to facilitate structural comparisons with the structures determined at lower pressure. Full crystallographic details are given in Table 1.

The atoms which become intercalated into the structure at 4.67 GPa were assigned as neon as this is was the hydrostatic medium used and it was surrounding the crystal. During review, it was suggested that the atoms may be oxygen, arising from ingress of water. This hypothesis can be ruled out on the following basis:

1. Prior to loading with neon the crystal was exposed to high vacuum in the gas-loader. This would have had a drying effect on the sample.
2. Any liquid water present in the sample would likely have crystallised as strongly scattering ice at *ca* 1 GPa (we have seen phase VI previously under these conditions) and been visible in the diffraction patterns.
3. The neon atoms are located in hydrophobic regions of the structure, and would be expected to H-bond to each other if they were in reality water, aqueous OH and O being the best donor/acceptor pair in the postulated structure. In the crystal structure at 4.46 GPa the only Ne...Ne distance less than 3 Å is between two symmetry-equivalent Ne4 sites, 2.57 Å. Although this is a plausible distance for the O...O interaction in a water dimer, it is a discrete interaction, with no further links made to other neon atoms. The next shortest distance is 3.26 Å between Ne1 and Ne2. This pattern of contacts is not what would be anticipated in a hydrate of Cu₂(L).
4. Finally if the Ne atoms are re-assigned as oxygen, and the structure re-refined, R_1 increases from 8.03 to 8.66%.

Calculation of Molecular Volumes

The molecular volumes of the pacman complexes were calculated via void volumes obtained using MERCURY.¹⁴ Neon atoms were removed prior to calculations in the neon-containing co-crystal structures. The calculations employed the contact surface algorithm which maps the entire void surface regardless of probe accessibility. The probe radius was 0.2 Å with a grid spacing of 0.1 Å (the minimum values allowed by the program). A chemically meaningful probe radius of 1.2 Å, representative of the radius of a molecule of H₂, was also tested but resulted in zero accessible volume. The interstitial void volumes reported here are not solvent accessible. The void volumes enable the molecular volumes of the pacman complex to be calculated according to [total unit cell volume – void volume]/Z. Void and molecular volumes are given in Table 2.

Other Programs Used

PIXEL packing energy calculations were carried out using CLP-PIXEL.¹⁵⁻¹⁶ Molecular electron densities were calculated using GAUSSIAN09¹⁷ with the B3LYP/6-31G** level of theory and basis set. CH distances were reset to 1.083 Å prior to the electron density calculations. The electron density was calculated in steps of 0.08 Å, with a condensation level of 5 used for the energy calculations. Equations-of-state (EOS) were determined using EOSFit-7,¹⁸ and strain tensor calculations were performed using the program STRAIN.¹⁹⁻²⁰ Geometries were measured using DIAMOND²¹ and PLATON.²²

B. Supplementary Tables

Table S1 Experimental details. All structures are monoclinic, $C2/c$ with $Z = 8$. H-atom parameters were constrained. $T = 298$ K unless otherwise specified. $\lambda = 0.7749$ and 0.4959 Å for the ambient and high-pressure collections, respectively. Measurements at 2.01 and 2.52 GPa contain unit cell information only as detector saturation problems degraded the quality of the intensity measurements in these cases.

Pressure (GPa)	0.00	0.00 ($T = 100$ K)	1.30	2.01	2.52	3.46
Chemical formula	$C_{42}H_{40}Cu_2N_8$	$C_{42}H_{40}Cu_2N_8$	$C_{42}H_{40}Cu_2N_8$	$C_{42}H_{40}Cu_2N_8$	$C_{42}H_{40}Cu_2N_8$	$C_{42}H_{40}Cu_2N_8$
M_r	783.90	783.90	783.90	783.90	783.90	783.90
a, b, c (Å)	25.3657 (15), 9.9388 (6), 29.1779 (17)	25.1863 (18), 9.9249 (7), 28.570 (2)	24.808 (6), 9.6971 (12), 27.648 (3)	24.557 (3), 9.5814 (8), 27.013 (2)	24.4289 (17), 9.5291 (4), 26.7021 (10)	24.281 (3), 9.4519 (6), 26.2355 (15)
β (°)	92.788 (2)	91.745 (3)	92.073 (4)	91.877 (2)	91.748 (1)	91.553 (2)
V (Å ³)	7347.2 (8)	7138.5 (9)	6646.7 (19)	6352.4 (11)	6213.0 (6)	6018.8 (8)
μ (mm ⁻¹)	1.51	1.55	0.50	0.53	0.54	0.56
Crystal size (mm)	0.10 × 0.05 × 0.05	0.1 × 0.05 × 0.05	0.09 × 0.08 × 0.07	0.09 × 0.08 × 0.07	0.09 × 0.08 × 0.07	0.09 × 0.08 × 0.07
T_{min}, T_{max}	0.643, 0.746	0.644, 0.747	0.430, 0.744	0.6454, 0.7438	0.585, 0.744	0.619, 0.744
No. of measured, independent and observed [$I > 2\sigma(I)$] reflections	37975, 6712, 5654	64755, 14237, 11627	10411, 2283, 1617	7264, 1396, 1214	11548, 2468, 1896	12029, 2374, 2067
R_{int}	0.104	0.090	0.171	0.042	0.046	0.041
$(\sin \theta/\lambda)_{max}$ (Å ⁻¹)	0.603	0.781	0.588	0.500	0.625	0.625
$R[F^2 > 2\sigma(F^2)], wR(F^2), S$	0.076, 0.195, 1.03	0.054, 0.148, 1.05	0.099, 0.283, 1.04	N/A	N/A	0.048, 0.134, 1.10
No. of parameters	478	478	227	N/A	N/A	228
No. of restraints	0	0	52	N/A	N/A	52
$\Delta\rho_{max}, \Delta\rho_{min}$ (e Å ⁻³)	0.77, -0.65	0.92, -0.76	0.52, -0.71	N/A	N/A	0.67, -0.44

Table 1 Experimental details continued

Pressure (GPa)	4.67	5.17	5.81	6.90	8.13
Chemical formula	C ₄₂ H ₄₀ Cu ₂ N ₈ ·Ne _{3.5}	C ₄₂ H ₄₀ Cu ₂ N ₈ ·Ne _{3.5}	C ₄₂ H ₄₀ Cu ₂ N ₈ ·Ne _{3.5}	C ₄₂ H ₄₀ Cu ₂ N ₈ ·Ne _{3.5}	C ₄₂ H ₄₀ Cu ₂ N ₈ ·Ne _{3.5}
M_r	854.53	854.53	854.53	854.53	854.53
a, b, c (Å)	24.259 (6), 9.2882 (15), 26.841 (4)	24.215 (6), 9.2391 (16), 26.599 (5)	24.115 (4), 9.2099 (11), 26.461 (3)	23.997 (3), 9.1398 (8), 26.1160 (18)	23.811 (7), 9.0709 (19), 25.766 (5)
β (°)	84.039 (8)	84.042 (8)	83.888 (7)	83.750 (5)	83.532 (7)
V (Å ³)	6015 (2)	5919 (2)	5843.5 (13)	5693.8 (9)	5530 (2)
μ (mm ⁻¹)	0.57	0.58	0.59	0.60	0.62
Crystal size (mm)	0.09 × 0.08 × 0.07	0.09 × 0.08 × 0.07	0.09 × 0.08 × 0.07	0.09 × 0.08 × 0.07	0.09 × 0.08 × 0.07
T_{\min}, T_{\max}	0.463, 0.744	0.227, 0.744	0.647, 0.744	0.595, 0.744	0.187, 0.744
No. of measured, independent and observed [$I > 2\sigma(I)$] reflections	7250, 1840, 1294	10068, 2208, 1477	11494, 2463, 1778	11829, 2325, 1623	10611, 2272, 1285
R_{int}	0.118	0.072	0.105	0.093	0.104
$(\sin \theta/\lambda)_{\max}$ (Å ⁻¹)	0.588	0.625	0.625	0.625	0.625
$R[F^2 > 2\sigma(F^2)], wR(F^2), S$	0.080, 0.191, 1.09	0.050, 0.117, 0.95	0.070, 0.189, 0.98	0.079, 0.211, 0.96	0.065, 0.162, 0.92
No. of parameters	241	240	240	240	240
No. of restraints	52	52	52	52	52
$\Delta\rho_{\max}, \Delta\rho_{\min}$ (e Å ⁻³)	0.48, -0.49	0.43, -0.38	0.58, -0.75	0.77, -0.76	0.46, -0.38

Table S2 Molecular volumes, unit cell volumes and their respective void contents, of Cu-Pacman complexes at different pressures. Details of the method used for calculating these data are given under *Calculation of Molecular Volumes* in Section A.

Complex	Pressure (GPa)	V_{cell} (\AA^3)	V_{void} (\AA^3)	% Void	V_{mol}	Temperature (K)
[Cu ₂ (L)]	0.00	7138.5(9)	2171.55	30.4	620.85	100
	0.00	7347.2(8)	2412.46	32.8	616.84	298
	1.30	6646.7(19)	1665.61	25.1	622.65	298
	3.46	6018.8(8)	1068.7	17.8	618.65	298
[Cu ₂ (L)]·Ne _{3.5}	4.67	6015(2)	1127.51	18.7	610.96	298
	5.17	5919(2)	1053.94	17.8	608.96	298
	5.81	5843.5(13)	998.13	17.1	605.67	298
	6.90	5693.8(9)	886.76	15.6	600.90	298
	8.13	5530(2)	771.24	13.9	594.81	298

C. Supplementary Figures

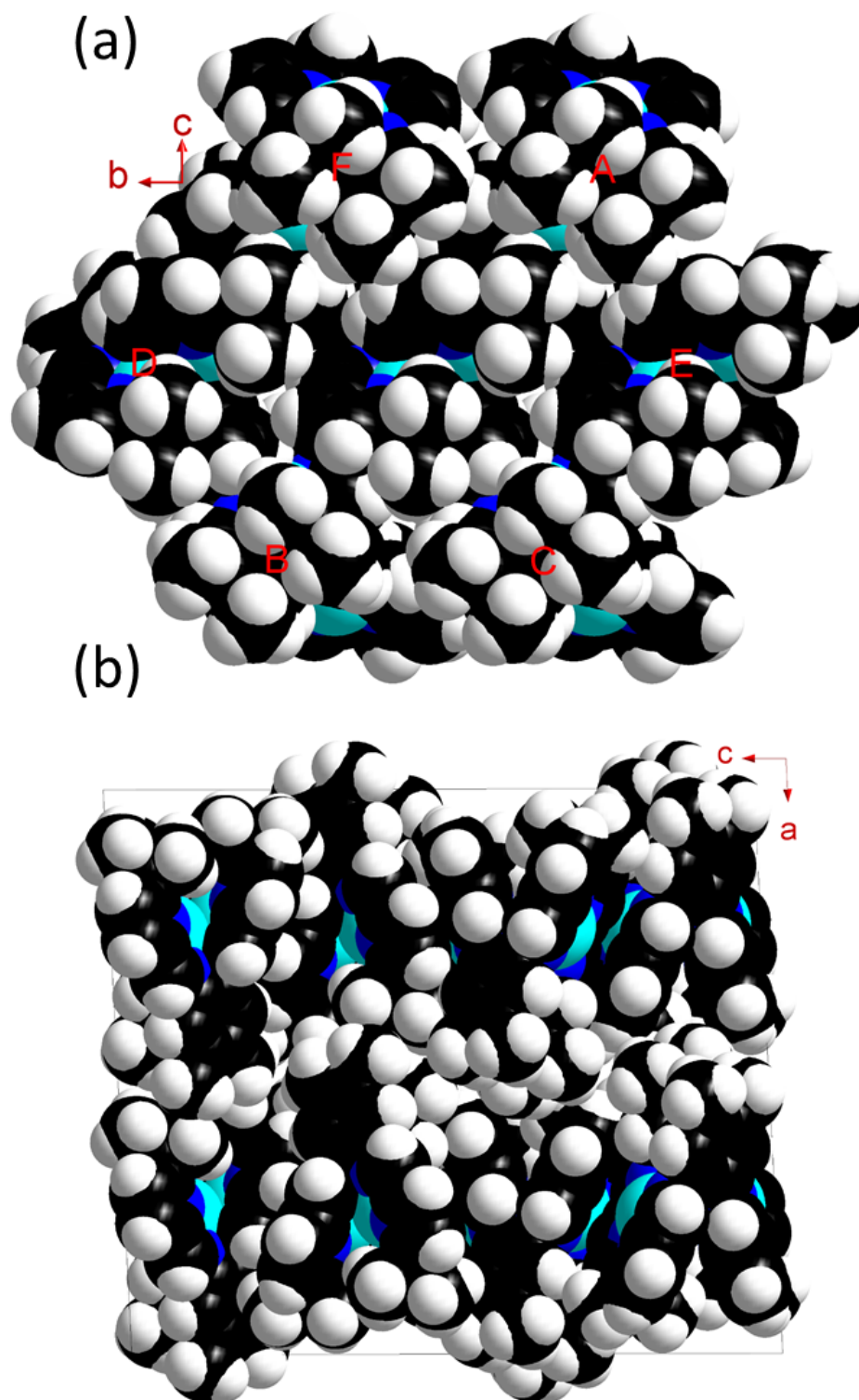


Figure S1 (a) The six strongest molecular contacts surrounding the central reference molecule are labelled A–F and (b) layered stacking along a. This is a copy of Fig. 2 in the main paper with the atoms shown in space-filling format to show the non porosity of the crystal structure.

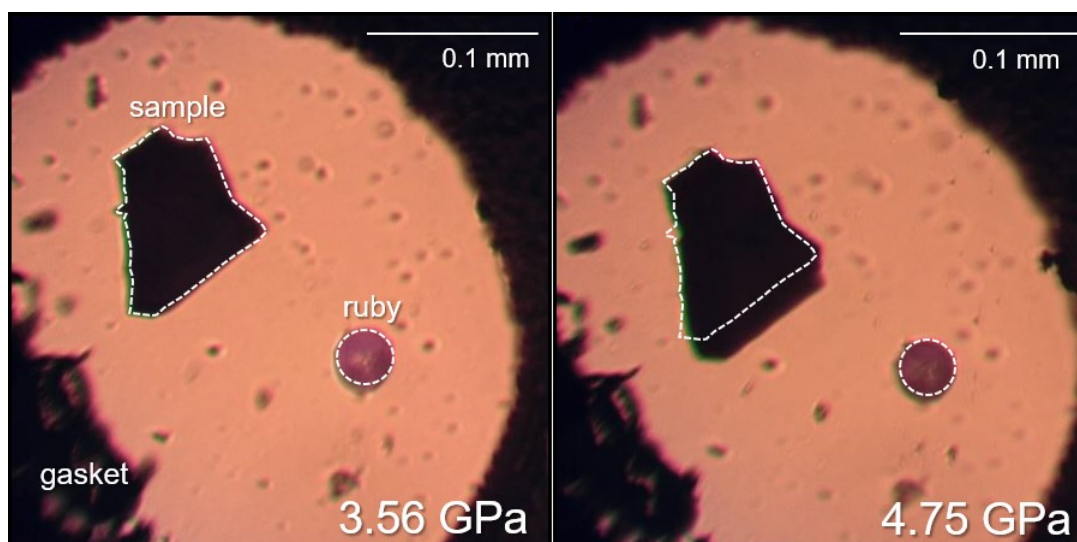


Figure S2. The contents of the DAC before and after neon freezing. The outline of the crystal and the ruby sphere prior to neon freezing (white dashed line) is superimposed on the post neon freezing image to highlight the change in crystal size and shape.

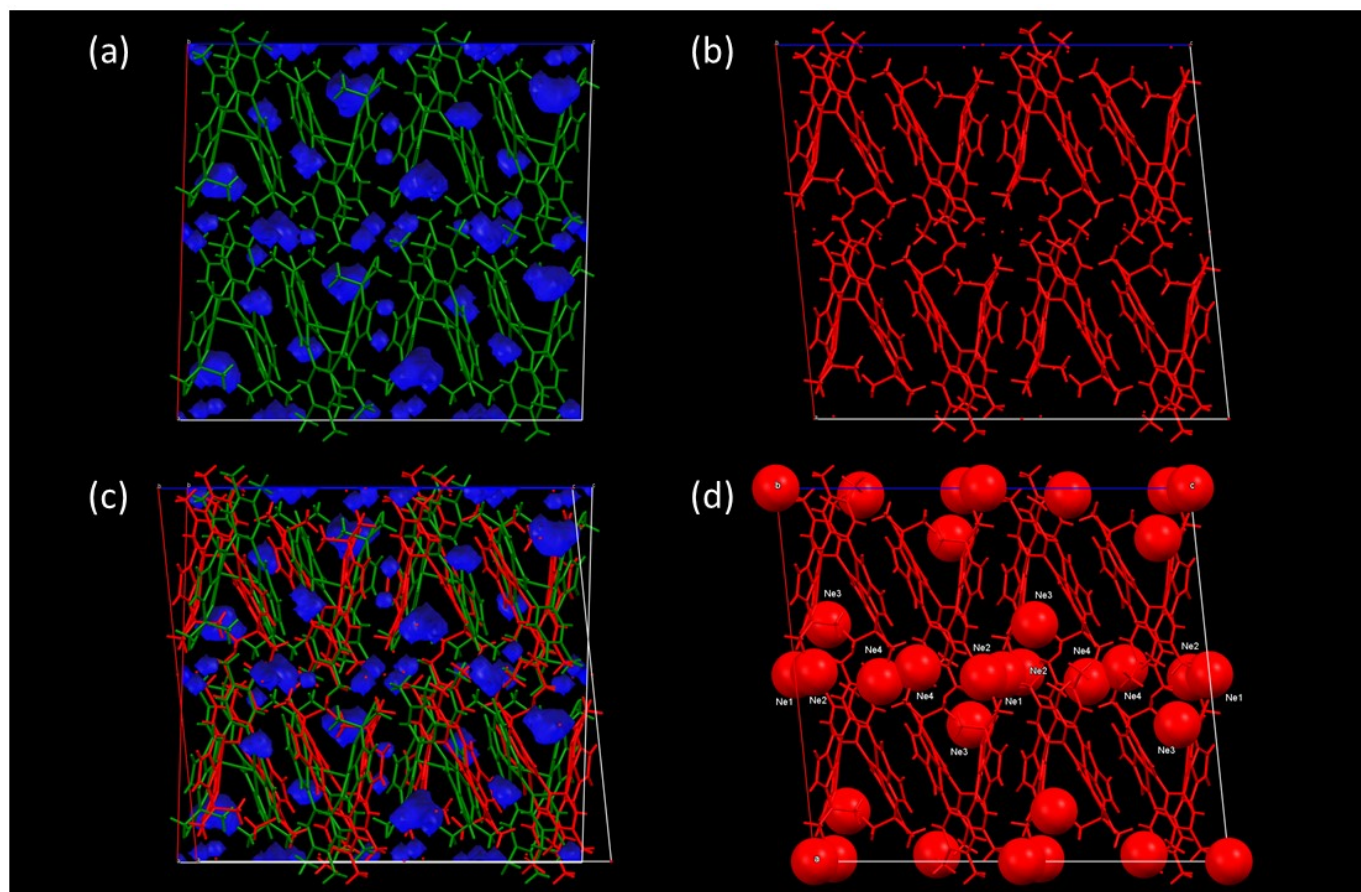


Figure S3 (a) The crystal structure of $\text{Cu}_2(\text{L})$ at 3.46 GPa. The figure was prepared in *Mercury* with a probe radius of 0.6 Å and a grid spacing of 0.3 Å. The default values of these parameters suitable for finding solvent-accessible voids are 1.2 and 0.7 Å, respectively, but no void space is found using these settings. (b) The crystal structure of $\text{Cu}_2(\text{L}).3.5\text{Ne}$ at 4.67 GPa. (c) Superposition of (a) and (b). (d) As (b) with the Ne drawn in space filling mode assuming a van der Waals radius of 1.54 Å. This value is taken from Bondi's compilation, a more recent estimate by Alvarez is 1.58 Å.

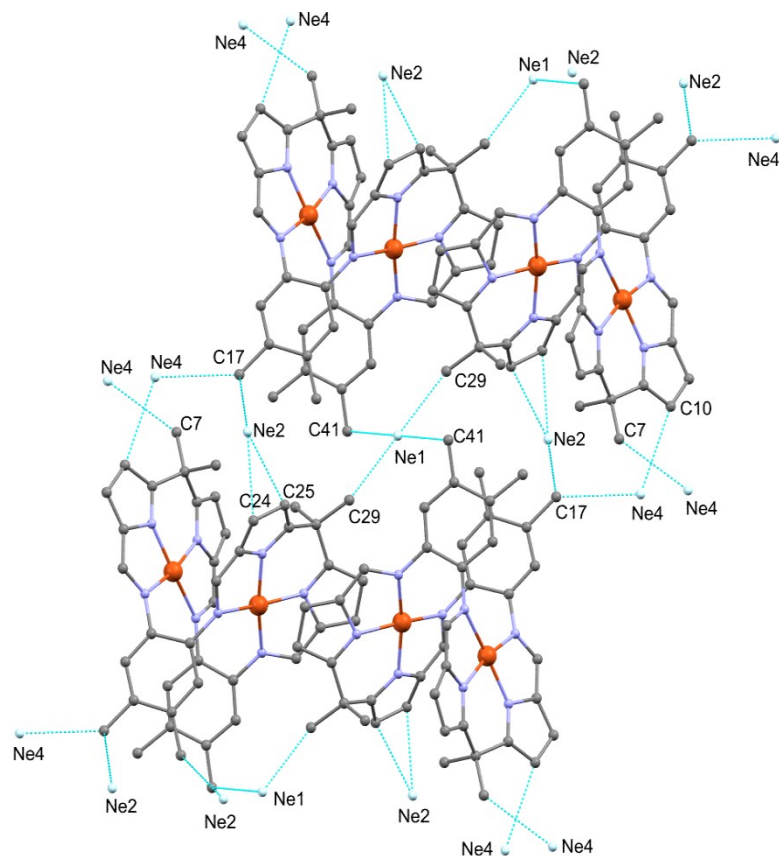


Figure S4 Neon atoms (1, 2, and 4) situated between the layers of pacman molecules at 4.67 GPa. Hydrogen atoms are omitted for clarity.

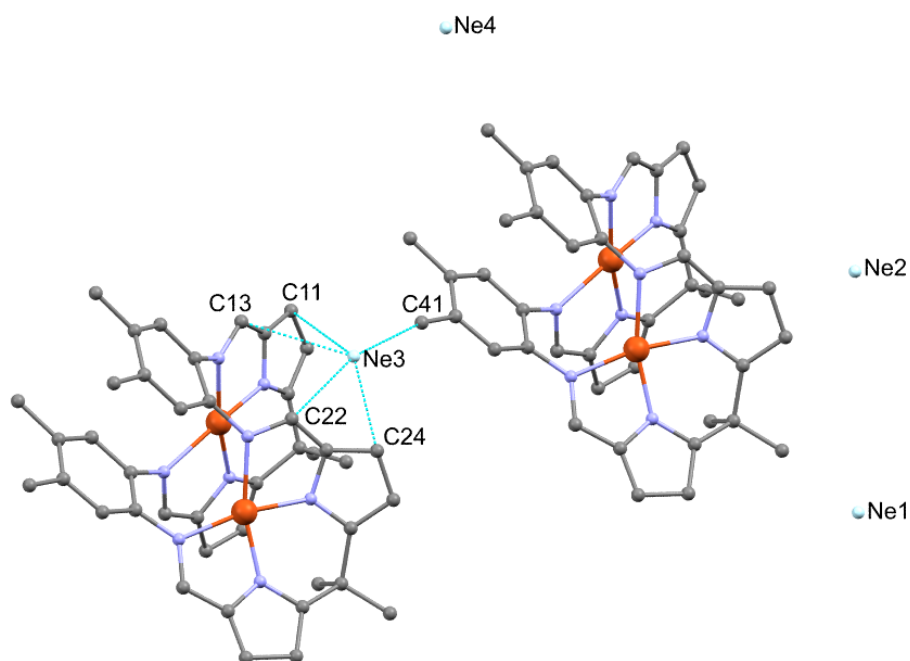


Figure S5 The Ne3...C shortest contacts (less than 3 Å) within the macrocyclic layers at 4.67 GPa. Hydrogen atoms are omitted for clarity.

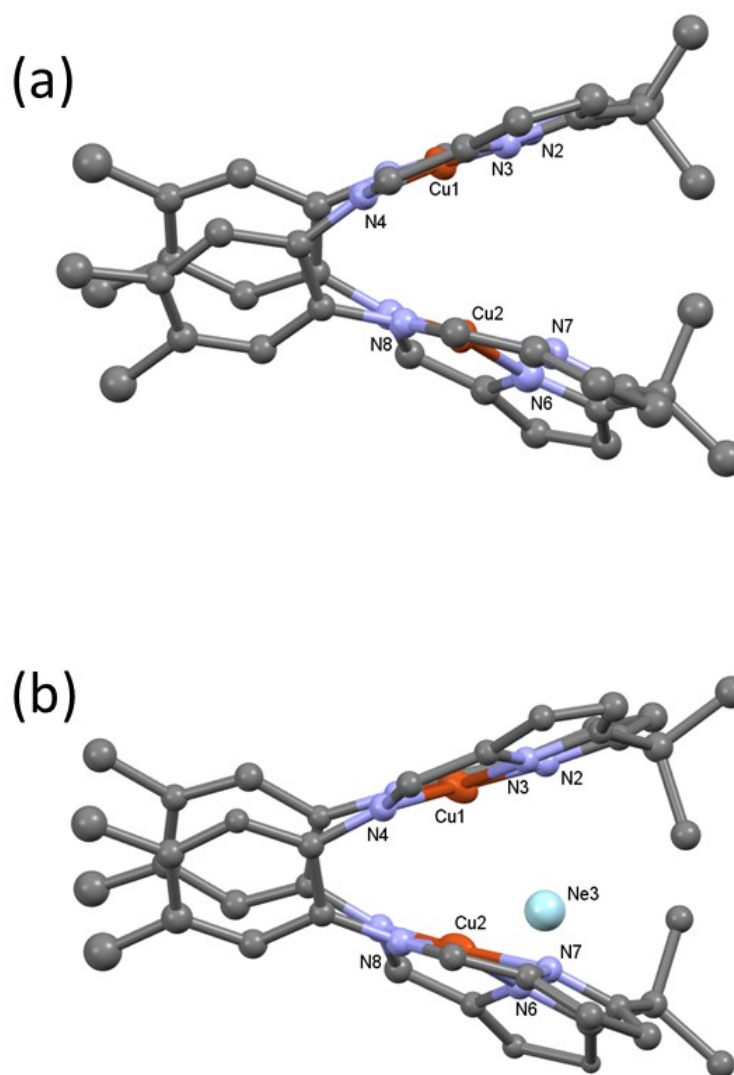


Figure S6 A view of the pacman complex **(a)** at 3.46 GPa before the phase transition and **(b)** just after the transition at 4.67 GPa.

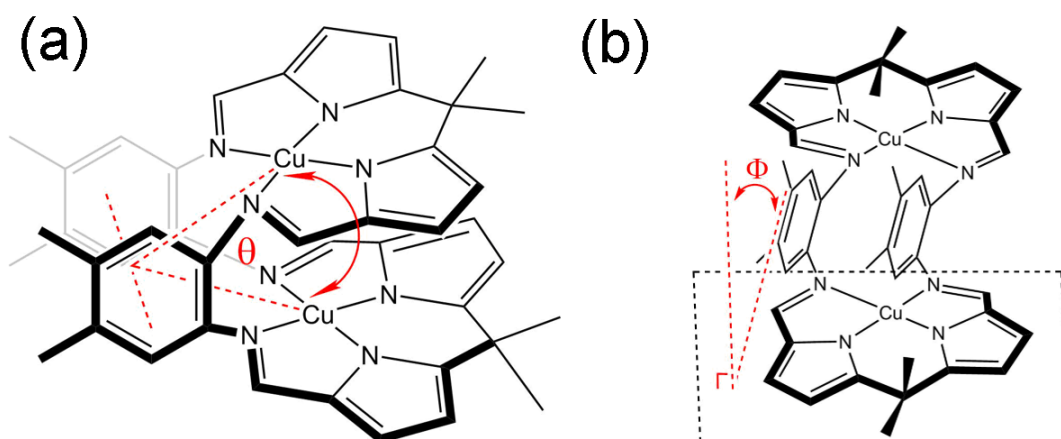


Figure S7 (a) the bite angle Θ and (b) the twist angle Φ . Figure adapted from Stevens et al.¹ The angles were calculated in the program DIAMOND.

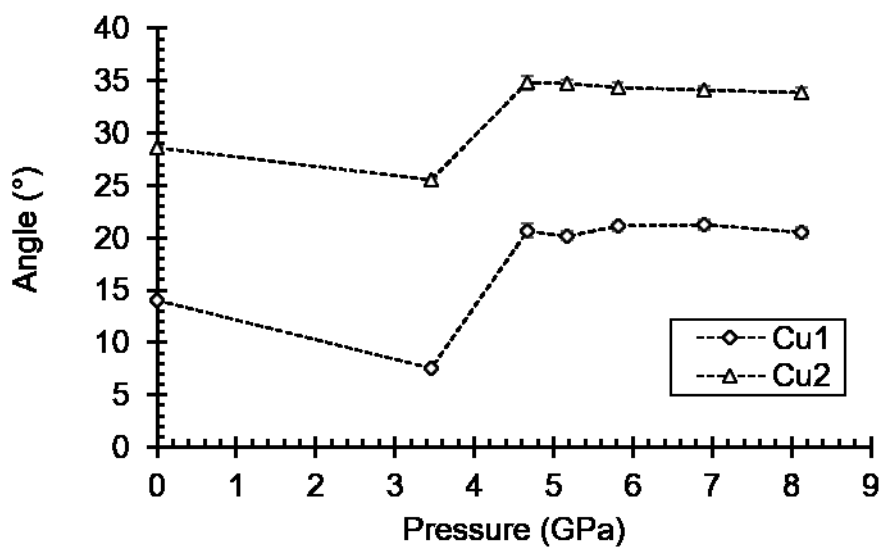


Figure S8: Variations in the interplanar angles between the two pyrrole based halves of the macrocyclic pockets for Cu1 and Cu2. The planes about Cu 1 are defined by atoms [N1, N2, C1-C5] and [N3, N4, C9-C13]. Those about Cu2 are defined by [N5, N6, C30-C34] and [N7, N8, C22-26].

References

1. Stevens, C. J.; Prescimone, A.; Tuna, F.; McInnes, E. J. L.; Parsons, S.; Morrison, C. A.; Arnold, P. L.; Love, J. B., Inter- versus Intramolecular Structural Manipulation of a Dichromium(II) Pacman Complex through Pressure Variation. *Inorg. Chem.* **2016**, *55* (1), 214-220.
2. Givaja, G.; Volpe, M.; Leeland, J. W.; Edwards, M. A.; Young, T. K.; Darby, S. B.; Reid, S. D.; Blake, A. J.; Wilson, C.; Wolowska, J.; McInnes, E. J. L.; Schröder, M.; Love, J. B., Design and Synthesis of Binucleating Macrocyclic Clefs Derived from Schiff - Base Calixpyrroles. *Chem. Eur. J.* **2007**, *13* (13), 3707-3723.
3. Thompson, A. C.; Padmore, H. A.; Oliver, A. G.; Teat, S. J.; Celestre, R. S.; Clark, S. M.; Domning, E. E.; Franck, K. D.; Morrison, G. Y., A Simple High Performance Beamline for Small Molecule Chemical Crystallography. *AIP Conference Proceedings* **2004**, *705* (1), 482-485.
4. Kunz, M.; MacDowell, A. A.; Caldwell, W. A.; Cambie, D.; Celestre, R. S.; Domning, E. E.; Duarte, R. M.; Gleason, A. E.; Glossinger, J. M.; Kelez, N.; Plate, D. W.; Yu, T.; Zaug, J. M.; Padmore, H. A.; Jeanloz, R.; Alivisatos, A. P.; Clark, S. M., A beamline for high-pressure studies at the Advanced Light Source with a superconducting bending magnet as the source. *J. Synchrotron Rad.* **2005**, *12* (5), 650-658.
5. Mao, H.; Xu, J.-A.; Bell, P., Calibration of the ruby pressure gauge to 800 kbar under quasi - hydrostatic conditions. *J. Geophys. Res: Solid Earth* **1986**, *91* (B5), 4673-4676.
6. *Apex 3, Bruker, Bruker AXS Inc., Madison, Wisconsin, USA, 2017.*
7. Tu, M.; Wiktor, C.; Rosler, C.; Fischer, R. A., Rapid room temperature syntheses of zeolitic-imidazolate framework (ZIF) nanocrystals. *Chem. Comm.* **2014**, *50* (87), 13258-13260.
8. Parsons, S., ECLIPSE- Program for masking high-pressure diffraction images and conversion between CCD image formats. The University of Edinburgh. **2014**.
9. *SADABS, Bruker, Bruker AXS Inc., Madison, Wisconsin, USA, 2014/15.*
10. Sheldrick, G. M. *XPREP*, 2008/2; Bruker, Bruker AXS Inc.: Madison, Wisconsin, USA, 2008.
11. Sheldrick, G., SHELXT - Integrated space-group and crystal-structure determination. *Acta Cryst.* **2015**, *A71* (1), 3-8.
12. Sheldrick, G., Crystal structure refinement with SHELXL. *Acta Cryst.* **2015**, *C71* (1), 3-8.
13. Dolomanov, O. V.; Bourhis, L. J.; Gildea, R. J.; Howard, J. A. K.; Puschmann, H., OLEX2: a complete structure solution, refinement and analysis program. *J. Appl. Cryst.* **2009**, *42* (2), 339-341.
14. Macrae, C. F.; Bruno, I. J.; Chisholm, J. A.; Edgington, P. R.; McCabe, P.; Pidcock, E.; Rodriguez-Monge, L.; Taylor, R.; van de Streek, J.; Wood, P. A., Mercury CSD 2.0 - new features for the visualization and investigation of crystal structures. *J. Appl. Cryst.* **2008**, *41* (2), 466-470.
15. Gavezzotti, A., Calculation of lattice energies of organic crystals: The PIXEL integration method in comparison with more traditional methods. *Z. Krist.* **2005**, *220*, 499-510.
16. Gavezzotti, A., Efficient computer modeling of organic materials. The atom-atom, Coulomb-London-Pauli (AA-CLP) model for intermolecular electrostatic-polarization, dispersion and repulsion energies. *New J. Chem.* **2011**, *35* (7), 1360-1368.
17. Frisch, M. J.; Trucks, G. W.; Schlegel, H. B.; Scuseria, G. E.; Robb, M. A.; Cheeseman, J. R.; Scalmani, G.; Barone, V.; Petersson, G. A.; Nakatsuji, H.; Li, X.; Caricato, M.; Marenich, A.; Bloino, J.; Janesko, B. G.; Gomperts, R.; Mennucci, B.; Hratchian, H. P.; Ortiz, J. V.;

Izmaylov, A. F.; Sonnenberg, J. L.; Williams-Young, D.; Ding, F.; Lipparini, F.; Egidi, F.; Goings, J.; Peng, B.; Petrone, A.; Henderson, T.; Ranasinghe, D.; Zakrzewski, V. G.; Gao, J.; Rega, N.; Zheng, G.; Liang, W.; Hada, M.; Ehara, M.; Toyota, K.; Fukuda, R.; Hasegawa, J.; Ishida, M.; Nakajima, T.; Honda, Y.; Kitao, O.; Nakai, H.; Vreven, T.; Throssell, K.; Jr., J. A. M.; Peralta, J. E.; Ogliaro, F.; Bearpark, M.; Heyd, J. J.; Brothers, E.; Kudin, K. N.; Staroverov, V. N.; Keith, T.; Kobayashi, R.; Normand, J.; Raghavachari, K.; Rendell, A.; Burant, J. C.; Iyengar, S. S.; Tomasi, J.; Cossi, M.; Millam, J. M.; Klene, M.; Adamo, C.; Cammi, R.; Ochterski, J. W.; Martin, R. L.; Morokuma, K.; Farkas, O.; Foresman, J. B.; Fox, D. J. *Gaussian 09, Revision E.01.*, Gaussian, Inc.: Wallingford CT, 2016.

18. Angel, R. J.; Alvaro, M.; Gonzalez-Platas, J., EosFit7c and a Fortran module (library) for equation of state calculations. *Z. Krist.* **2014**, *229* (5), 405.

19. Parsons, S. *STRAIN: Calculation of Strain Tensor*, 10; The University of Edinburgh, 2003.

20. Ohashi, Y.; Burnham, C. W., Clinopyroxene lattice deformations. Roles of chemical substitution and temperature. *American Mineralogist* **1973**, *58* (9-10), 843-849.

21. Bradenburg K., B. M. *DIAMOND Version 2.1. Crystal Impact GbR, Bonn, Germany*, 2001.

22. Spek, A., Structure validation in chemical crystallography. *Acta Cryst.* **2009**, *D65* (2), 148-155.